



HAL
open science

Stray field computation by inverted finite elements: a new method in micromagnetic simulations

Tahar Z. Boulmezaoud, Keltoum Kaliche

► To cite this version:

Tahar Z. Boulmezaoud, Keltoum Kaliche. Stray field computation by inverted finite elements: a new method in micromagnetic simulations. *Advances in Computational Mathematics*, 2024, 50 (3), 10.1007/s10444-024-10139-2 . hal-04683702

HAL Id: hal-04683702

<https://hal.science/hal-04683702>

Submitted on 2 Sep 2024

HAL is a multi-disciplinary open access archive for the deposit and dissemination of scientific research documents, whether they are published or not. The documents may come from teaching and research institutions in France or abroad, or from public or private research centers.

L'archive ouverte pluridisciplinaire **HAL**, est destinée au dépôt et à la diffusion de documents scientifiques de niveau recherche, publiés ou non, émanant des établissements d'enseignement et de recherche français ou étrangers, des laboratoires publics ou privés.

Stray field computation by inverted finite elements: a new method in micromagnetic simulations

Tahar Z. BOULMEZAOUD^{1,2,3} and Keltoum KALICHE^{1,3}

ABSTRACT. In this paper, we propose a new method for computing the stray-field and the corresponding energy for a given magnetization configuration. Our approach is based on the use of inverted finite elements and does not need any truncation. After analyzing the problem in an appropriate functional framework, we describe the method and we prove its convergence. We then display some computational results which demonstrate its efficiency and confirm its full potential.

1. INTRODUCTION

In micromagnetics, the structure of a magnetic body $\Omega \subset \mathbb{R}^3$ is often described by the magnetization \mathbf{M} , which is a vector field defined over Ω and minimizing the Landau-Lifschitz functional. In terms of dimensionless variables, the latter energy can be written into the form

$$\mathcal{E}(\mathbf{M}) = \alpha \int_{\Omega} |\nabla \mathbf{M}|^2 + \int_{\Omega} \varphi(\mathbf{M}) dx + \frac{1}{2} \int_{\mathbb{R}^3} |\nabla u|^2 dx - \int_{\mathbb{R}^3} \mathbf{H}_e \cdot \mathbf{M} dx,$$

where $\varphi \geq 0$ is a function describing the orientation of the magnetization, $\alpha > 0$ is a real parameter, \mathbf{H}_e the external magnetic field and u is magnetostatic potential. The latter quantity is related to the stray-field (or the magnetic induction) \mathbf{h} by

$$(1) \quad \mathbf{h} = -\nabla u.$$

The existence of the scalar potential u comes from Maxwell's equation

$$(2) \quad \operatorname{curl} \mathbf{h} = \mathbf{0} \text{ in } \mathbb{R}^3.$$

Moreover, the stray-field \mathbf{h} and the magnetization \mathbf{M} are related by the equation

$$(3) \quad \operatorname{div}(\mathbf{h} + \mathbf{M}\chi_{\Omega}) = 0 \text{ in } \mathbb{R}^3,$$

where χ_{Ω} stands for characteristic (or indicator) function of Ω . Rewriting (3) in terms of u and \mathbf{M} gives the well known equation

$$(4) \quad \Delta u = \operatorname{div}(\mathbf{M}\chi_{\Omega}) \text{ in } \mathbb{R}^3.$$

¹ Université Paris-Saclay, UVSQ, LMV, Versailles, France.

² Department of Mathematics and Statistics, University of Victoria, Victoria, British Columbia, Canada.

³ University Kasdi Merbeh, Ouargla, Algeria.

E-mail addresses: tahar.boulmezaoud@uvsq.fr, keltoumkaliche@yahoo.fr.

2020 Mathematics Subject Classification. 35Q60, 35A35, 65M99.

Key words and phrases. Inverted finite elements, micromagnetics, stray field, magnetostatics, unbounded domains.

This equation can also be written into the form

$$(5) \quad \left\{ \begin{array}{ll} \Delta u = \operatorname{div} \mathbf{M} & \text{in } \Omega, \\ \Delta u = 0 & \text{in } \mathbb{R}^3 \setminus \overline{\Omega}, \\ [u] = 0 & \text{on } \partial\Omega, \\ \left[\frac{\partial u}{\partial n} \right] = -\mathbf{M} \cdot \mathbf{n} & \text{on } \partial\Omega, \end{array} \right.$$

where \mathbf{n} is the exterior normal on $\partial\Omega$. In addition, the magnetization \mathbf{M} is subject to the Heisenberg-Weiss condition

$$(6) \quad |\mathbf{M}| \text{ is constant in } \Omega.$$

It is well known that calculating the stray-field \mathbf{h} and the corresponding energy

$$(7) \quad \mathcal{E}_{sf}(u) = \frac{1}{2} \int_{\mathbb{R}^3} |\mathbf{h}|^2 dx,$$

from the magnetization \mathbf{M} is one of the most important steps in studying micromagnetic configurations of a body Ω . We may observe that a consequence of identity (4) is that the stray-field energy also writes

$$(8) \quad \mathcal{E}_{sf}(u) = \frac{1}{2} \int_{\mathbb{R}^3} |\nabla u|^2 dx = -\frac{1}{2} \int_{\Omega} \mathbf{M} \cdot \mathbf{h} dx.$$

(see also the weak formulation of (4) hereafter).

In the existing litterature, one can find mainly two categories of methods. In the first category the calculation of u and \mathbf{h} is often based on solving the elliptic partial differential equation (4). In that case, the computational domain is often truncated and approximation is done in a sufficiently large bounded region (see, e. g., [3], [18], [10, 15], [6] and [21], [12] and [13]). In the second category of methods, the approach consists to evaluate u using the integral formula (see, e. g., [9])

$$(9) \quad u(\mathbf{x}) = \frac{1}{4\pi} \int_{\Omega} \frac{(\mathbf{x} - \mathbf{y}) \cdot \mathbf{M}(\mathbf{y})}{|\mathbf{y} - \mathbf{x}|^3} d\mathbf{y}.$$

Among methods using formula (9), one can mention methods based on the Fast Fourier transform and fast Multipole methods (see, e. g., [4], [17]), H -matrix techniques ([20]) or direct integration methods (see, e. g., [9], [16]).

In this paper, the focus is on computing the stray-field \mathbf{h} from the magnetization \mathbf{M} by a novel approach based on the use of inverted finite element method (IFEM). IFEM was first introduced by Boulmezaoud in [5] for solving elliptic problem in unbounded domains without any truncation. In the context of equation (4) considered here, the domain of computation \mathbb{R}^3 is considered in its entirety. The deployment of IFEM is based on a weak formulation of (4) in an appropriate weighted space.

The paper is organized as follows. In section 2, we employ some weighted function spaces to study equation (4), completed with asymptotic conditions when $|\mathbf{x}| \rightarrow +\infty$. In particular, we give some details about the behavior at large distances and about the smoothness of the solution and of its derivatives. Section 3 is devoted to an outline of IFEM. After giving the general lines of the method, we prove its convergence in the context of equation (4). In the last section, we give some numerical results obtained with a 3D code.

2. PRELIMINARIES. WELL POSEDNESS OF THE PROBLEM

In the sequel, Ω denotes an open and connected subset of \mathbb{R}^3 having a lipschitzian boundary, not necessarily bounded (althought in physical applications Ω is often a bounded domain). Let \mathbf{M} be a vector field defined over Ω . From a strictl mathematical point, unless otherwise indicated, we only assume that

$$(10) \quad \int_{\Omega} |\mathbf{M}|^2 dx < \infty.$$

Assumption (10) is obviously valid when Ω is bounded (or has a finite volume) and when $|\mathbf{M}|$ is satisfying the Heisenberg-Weiss constraint (6). In that case

$$\|\mathbf{M}\|_{L^2(\Omega)^3}^2 = \int_{\Omega} |\mathbf{M}|^2 dx = |\mathbf{M}|^2 |\Omega| < +\infty.$$

We now come back to equation (4). Without going into the technicalities of Poisson equation, it can be seen that existence and uniqueness of solutions to (4) depend on the required behavior at large distances, that is when $|\mathbf{x}| \rightarrow +\infty$. To illustrate this, one may observe that polynomial growth of solutions at large distances should be excluded, otherwise uniqueness may be lost since harmonic polynomials can be added to any solution of (4) (see, e. g., [11], [2]). Fortunately, in the current context, u must fulfill the physical constraint

$$(11) \quad \int_{\mathbb{R}^3} |\nabla u|^2 dx < \infty,$$

which means that $\mathbf{h} = -\nabla u$ has a finite energy. In view of Hardy's inequality (see, e. g., [2]), it is natural to require that

$$(12) \quad \int_{\mathbb{R}^3} \frac{|u|^2}{|\mathbf{x}|^2 + 1} dx < \infty.$$

For this reason, we need to introduce some weighted function spaces. For all integers $\ell \geq 0$ and $m \geq 0$, $W_{\ell}^m(\mathbb{R}^3)$ stands for the space of all the functions satisfying

$$\forall |\lambda| \leq m, (1 + |\mathbf{x}|^2)^{(\ell+|\lambda|-m)/2} D^{\lambda} v \in L^2(\mathbb{R}^3).$$

This space is endowed with the norm

$$(13) \quad \|v\|_{W_{\ell}^m(\mathbb{R}^3)} = \left(\sum_{|\lambda| \leq m} \int_{\mathbb{R}^3} (|\mathbf{x}|^2 + 1)^{|\lambda|+\ell-m} |D^{\lambda} v|^2 dx \right)^{1/2}.$$

In other words, elements of $W_0^1(\mathbb{R}^3)$ are those functions satisfying (11) and (12). We may observe that non vanishing polynomial functions do not belong to $W_0^1(\mathbb{R}^3)$. Before continuing with problem (4), let us recall that for any function $v \in W_{\alpha}^1(\mathbb{R}^3)$, $\alpha \in \mathbb{R} \setminus \{-1/2\}$, one has (see, e. g., [1])

$$(14) \quad \lim_{|\mathbf{x}| \rightarrow +\infty} |\mathbf{x}|^{\alpha+1/2} \|u(|\mathbf{x}|, \cdot)\|_{L^2(\mathbb{S}^2)} = 0,$$

where \mathbb{S}^2 is the unit sphere of \mathbb{R}^3 and

$$(15) \quad \|u(|\mathbf{x}|, \cdot)\|_{L^2(\mathbb{S}^2)}^2 = \int_{\mathbb{S}^2} |u(|\mathbf{x}|, \sigma)|^2 d\sigma.$$

Equation (4), completed with asymptotic conditions (11) and (12), can be written into the variational form: find $u \in W_0^1(\mathbb{R}^3)$ such that

$$(16) \quad \forall v \in W_0^1(\mathbb{R}^3), \int_{\mathbb{R}^3} \nabla u \cdot \nabla v dx = \int_{\Omega} \mathbf{M} \cdot \nabla v dx.$$

We have the following result

Proposition 2.1 (Well posedness). *Suppose that assumption (10) holds true. Then, (16), and consequently (4), has one and only one solution in $W_0^1(\mathbb{R}^3)$. Moreover, the following estimates hold*

$$(17) \quad \|(|\mathbf{x}|^2 + 1)^{-1/2}u\|_{L^2(\mathbb{R}^3)} \leq 2\|\mathbf{M}\|_{L^2(\Omega)},$$

$$(18) \quad \|\nabla u\|_{L^2(\mathbb{R}^3)^3} \leq \|\mathbf{M}\|_{L^2(\Omega)}.$$

We should note immediately that the decay of u at large distances is faster than in estimates (17) and (18). Actually, $u \in L^2(\mathbb{R}^3)$ and $(|\mathbf{x}|^2 + 1)^{1/2}\nabla u \in L^2(\mathbb{R}^3)^3$ as it will be stated in Proposition 2.2 hereafter.

PROOF OF PROPOSITION 2.1 – Let us first recall the classical Hardy inequality

$$(19) \quad \forall v \in \mathcal{D}(\mathbb{R}^3), \int_{\mathbb{R}^3} \frac{|u|^2}{|\mathbf{x}|^2} dx \leq 4 \int_{\mathbb{R}^3} |\nabla u|^2 dx.$$

Thus,

$$(20) \quad \forall v \in \mathcal{D}(\mathbb{R}^3), \int_{\mathbb{R}^3} \frac{|u|^2}{|\mathbf{x}|^2 + 1} dx \leq 4 \int_{\mathbb{R}^3} |\nabla u|^2 dx.$$

By density of $\mathcal{D}(\mathbb{R}^3)$ in $W_0^1(\mathbb{R}^3)$ (see [14]), the last inequality remains valid for $v \in W_0^1(\mathbb{R}^3)$. It follows that the bilinear form on the left hand side of (16) is coercive. The linear form on the right hand side of (16) satisfies

$$\left| \int_{\Omega} \mathbf{M} \cdot \nabla v dx \right| \leq \|\mathbf{M}\|_{L^2(\Omega)^3} \cdot \|\nabla v\|_{L^2(\mathbb{R}^3)^3}.$$

Existence and uniqueness follow from Lax-Milgram theorem. Moreover, taking $v = u$ in (16) gives estimate (18). Combining with inequality (20) gives (17). ■

Since the right hand side of (16) is in a divergence form, we also get the following result

Proposition 2.2 (Asymptotic behavior). *Let $u \in W_0^1(\mathbb{R}^3)$ be solution of (4). Then,*

- (1) $u \in L^2(\mathbb{R}^3)$,
- (2) $(1 + |\mathbf{x}|^2)^{1/2}\nabla u \in L^2(\mathbb{R}^3)^3$.
- (3) $\lim_{|\mathbf{x}| \rightarrow +\infty} |\mathbf{x}|^{3/2}\|u(|\mathbf{x}|, \cdot)\|_{L^2(\mathbb{S}^2)} = 0$ where $\|u(|\mathbf{x}|, \cdot)\|_{L^2(\mathbb{S}^2)}$ is defined by (15).

PROOF OF PROPOSITION (2.2) – Let us prove that $u \in W_1^1(\mathbb{R}^3)$. This is a direct consequence of the following lemma which is a particular case of a more general result proven in [2] (Theorem 2.16):

Lemma 2.3. *Let $m \geq 0$ be an integer. Then, the Laplace operator*

$$\Delta : W_{m+1}^{m+1}(\mathbb{R}^3) \mapsto W_{m+1}^{m-1}(\mathbb{R}^3) \perp \mathbb{R}$$

is an isomorphism.

Here $W_1^{-1}(\mathbb{R}^3)$ stands for the dual space of $W_{-1}^1(\mathbb{R}^3)$. It may be noted at this point that constant functions belong to $W_{-1}^1(\mathbb{R}^3)$. By $W_1^{-1}(\mathbb{R}^3) \perp \mathbb{R}$ we mean the space of functions $f \in W_1^{-1}(\mathbb{R}^3)$ satisfying

$$(21) \quad \langle f, 1 \rangle_{W_1^{-1}(\mathbb{R}^3), W_{-1}^1(\mathbb{R}^3)} = 0.$$

In the context of equation (4), the right hand side is $f = \operatorname{div}(\mathbf{M}\chi_\Omega)$. Thus, $f \in W_1^{-1}(\mathbb{R}^3)$ (since, obviously, $\mathbf{M}\chi_\Omega \in W_1^0(\mathbb{R}^3)^3$) and (21) is automatically fulfilled. We conclude that $u \in W_1^1(\mathbb{R}^3)$, thanks to Lemma 2.3. This ends the proof of the two first assertions. The third assertion follows from property (14). ■

REMARK – One can also prove that $u \in L^2(\mathbb{R}^3)$ by means of the Fourier transform.

Proposition 2.4 (Regularity). *Assume that Ω is a bounded open set of \mathbb{R}^3 with a $\mathcal{C}^{1,1}$ boundary and that*

$$(22) \quad \mathbf{M} \in L^2(\Omega)^3, \operatorname{div} \mathbf{M} \in L^2(\Omega) \text{ and } \mathbf{M} \cdot \mathbf{n} \in H^{1/2}(\partial\Omega).$$

Let $u \in W_0^1(\mathbb{R}^3)$ be solution of (4). Then,

- (1) $u|_\Omega \in H^2(\Omega)$,
- (2) $u|_{\mathbb{R}^3 \setminus \bar{\Omega}} \in W_2^2(\mathbb{R}^3 \setminus \bar{\Omega})$, that is

$$\forall 1 \leq i, j \leq 3, (|\mathbf{x}|^2 + 1) \frac{\partial^2 u}{\partial x_i \partial x_j} \in L^2(\mathbb{R}^3 \setminus \bar{\Omega}).$$

- (c) If $\mathbf{M} \cdot \mathbf{n} = 0$ on $\partial\Omega$, then $u \in W_2^2(\mathbb{R}^3)$.

PROOF OF PROPOSITION (2.4). – Let $u_0 \in H^2(\Omega)$ such that

$$u_0 = 0 \text{ and } \frac{\partial u_0}{\partial n} = \mathbf{M} \cdot \mathbf{n} \text{ on } \partial\Omega.$$

Set

$$U = \begin{cases} u - u_0 & \text{in } \Omega, \\ u & \text{in } \mathbb{R}^3 \setminus \bar{\Omega}. \end{cases}$$

Since $[U] = 0$ on $\partial\Omega$, we easily deduce that $U \in W_0^1(\mathbb{R}^3)$. Moreover, we have

$$\left[\frac{\partial U}{\partial n} \right] = 0 \text{ on } \partial\Omega,$$

Thus,

$$\Delta U = (\operatorname{div} \mathbf{M} - \Delta u_0)\chi_\Omega \in W_2^0(\mathbb{R}^3).$$

The right hand side of this equation satisfies

$$\langle \operatorname{div} \mathbf{M} - \Delta u_0, 1 \rangle = \int_\Omega \operatorname{div}(\mathbf{M} - \nabla u_0) dx = \int_\Omega (\mathbf{M} \cdot \mathbf{n} - \frac{\partial u_0}{\partial n}) d\sigma = 0.$$

In view of Lemma 2.3, we deduce that $U \in W_2^2(\mathbb{R}^3)$. By restricting to Ω and to $\mathbb{R}^3 \setminus \bar{\Omega}$ we get $u|_\Omega = U|_\Omega + u_0 \in H^2(\Omega)$ and $u|_{\mathbb{R}^3 \setminus \bar{\Omega}} = U|_{\mathbb{R}^3 \setminus \bar{\Omega}} \in W_2^2(\mathbb{R}^3 \setminus \bar{\Omega})$. Suppose now that $\mathbf{M} \cdot \mathbf{n} = 0$ on $\partial\Omega$. Then, $\operatorname{div}(\mathbf{M}\chi_\Omega) \in L^2(\mathbb{R}^3)$. Since $\operatorname{div}(\mathbf{M}\chi_\Omega) = 0$ in $\mathbb{R}^2 \setminus \bar{\Omega}$, we also deduce that $\operatorname{div}(\mathbf{M}\chi_\Omega) \in W_2^0(\mathbb{R}^3)$. In view of Lemma 2.3, we deduce that $u \in W_2^2(\mathbb{R}^3)$. This ends the proof of Proposition 2.4. ■

Let us finish this section with an observation. In view of equations (5) the potential u can be as written as

Proposition 2.5. *Suppose that $\mathbf{M} \in H(\operatorname{div}; \Omega)$. Let $u \in W_0^1(\mathbb{R}^3)$ be the unique solution of (4). Then,*

$$(23) \quad u = u_0 + u_1,$$

where $u_0 \in W_1^2(\mathbb{R}^3)$ is the unique solution of the Poisson equation

$$(24) \quad \Delta u_0 = \widetilde{\operatorname{div} \mathbf{M}} \text{ in } \mathbb{R}^3,$$

where $\widetilde{\operatorname{div} \mathbf{M}}$ designates the extension of $\operatorname{div} \mathbf{M}$ by zero outside Ω , while $u_1 \in W_0^1(\mathbb{R}^3)$ is the unique solution of the system

$$(25) \quad \int_{\mathbb{R}^3} \nabla u_1 \cdot \nabla v \, dv = \langle \mathbf{M} \cdot \mathbf{n}, v \rangle_{H^{-1/2}(\partial\Omega), H^{1/2}(\partial\Omega)}, \text{ for all } v \in W_0^1(\mathbb{R}^3).$$

Moreover, $u_0 \in W_2^2(\mathbb{R}^3)$ iff $\langle \mathbf{M} \cdot \mathbf{n}, 1 \rangle = 0$. In that case $u_1 \in W_1^1(\mathbb{R}^3)$.

Proof. Since $\operatorname{div} \mathbf{M} \in L^2(\Omega)$, $\widetilde{\operatorname{div} \mathbf{M}} \in L^2(\mathbb{R}^3) \hookrightarrow W_{-1}^0(\mathbb{R}^3)$. Following the same argument as in the proof Proposition 2.1, we easily deduce existence and uniqueness of u_0 and u_1 solutions of (24) and (25), respectively. From Lemma 2.3, we deduce that $u_0 \in W_2^2(\mathbb{R}^3)$ iff $\widetilde{\operatorname{div} \mathbf{M}} \in W_2^0(\mathbb{R}^3) \perp \mathbb{R}$, that is

$$\langle \mathbf{M} \cdot \mathbf{n}, 1 \rangle = \int_{\Omega} \operatorname{div} \mathbf{M} \, dx = 0.$$

Since $u \in W_1^1(\mathbb{R}^3)$ (see Proposition 2.2), we also have $u_1 = u - u_0 \in W_1^1(\mathbb{R}^3)$. \square

REMARK – Under assumptions of Proposition 2.5, we can write (see also, e. g., [9])

$$u = -\mathcal{N}(\operatorname{div} \mathbf{M}) + \mathcal{V}(\mathbf{M} \cdot \mathbf{n}),$$

where \mathcal{N} is the Newton potential defined by

$$\mathcal{N}w(\mathbf{x}) = \frac{1}{4\pi} \int_{\Omega} \frac{w(\mathbf{y})}{|\mathbf{x} - \mathbf{y}|} \, d\mathbf{y},$$

while \mathcal{V} is the single layer potential defined by

$$\mathcal{V}\phi(\mathbf{x}) = \int_{\partial\Omega} \frac{\phi(\mathbf{y})}{|\mathbf{x} - \mathbf{y}|} \, d\sigma(\mathbf{y}).$$

When $\langle \mathbf{M} \cdot \mathbf{n}, 1 \rangle \neq 0$, $\mathcal{N}(\operatorname{div} \mathbf{M})$ and $\mathcal{V}(\mathbf{M} \cdot \mathbf{n})$ decreases more slowly than u when $|\mathbf{x}| \rightarrow +\infty$. In fact, in view of Proposition 2.5, $u_0 = -\mathcal{N}(\operatorname{div} \mathbf{M}) \in W_1^2(\mathbb{R}^3) \hookrightarrow W_0^1(\mathbb{R}^3)$ and $u_1 = \mathcal{V}(\mathbf{M} \cdot \mathbf{n}) \in W_0^1(\mathbb{R}^3)$ while $u_{\mathbb{R}^3 \setminus \bar{\Omega}} \in W_2^2(\mathbb{R}^3 \setminus \bar{\Omega}) \hookrightarrow L^2(\mathbb{R}^3 \setminus \bar{\Omega})$. Indeed, when \mathbf{M} is sufficiently smooth, we have

$$|u_0(\mathbf{x})| = O\left(\frac{1}{|\mathbf{x}|}\right), \quad |u_1(\mathbf{x})| = O\left(\frac{1}{|\mathbf{x}|}\right), \quad \text{when } |\mathbf{x}| \rightarrow +\infty,$$

while, in view of formula (9), we have

$$|u(\mathbf{x})| = O\left(\frac{1}{|\mathbf{x}|^2}\right), \quad \text{when } |\mathbf{x}| \rightarrow +\infty.$$

At this stage, mathematical aspects concerning equation (4) are prepared. It remains to show the way in which this problem is discretized by inverted finite elements method. This will be done in the next section.

3. INVERTED FINITE ELEMENTS METHOD

Inverted finite elements method was developed by Boulmezaoud [5]. We will tailor it here for solving problem (4). The starting point consists to partition the whole space \mathbb{R}^3 into two subdomains

$$(26) \quad \mathbb{R}^3 = \overline{\Omega}_0 \cup \overline{\Omega}_\infty.$$

Here Ω_0 is bounded region while Ω_∞ is an unbounded one. We should note immediately that the bounded Ω_0 is not intended to be large. In particular, we do not rule out the possibility that $\Omega_0 = \emptyset$ and $\Omega_\infty = \mathbb{R}^3$. However, the following constraint is imposed to Ω_∞ (or, indirectly, to $\Omega_0 = \mathbb{R}^3 \setminus \overline{\Omega}_\infty$): Ω_∞ is the non-overlapping union of a finite number of infinite tetrahedra, that is

$$(27) \quad \overline{\Omega}_\infty = T_1 \cup T_2 \cup \dots \cup T_M,$$

with T_1, \dots, T_M , $M \geq 1$, are M infinite tetrahedra satisfying the assumptions

- T_1, \dots, T_M have a common fictitious vertex. Subsequently, we assume that this common fictitious vertex is the origin.
- the intersection of two arbitrary infinite tetrahedra T_i and T_j , $1 \leq i < j \leq M$, is either the empty set, a whole edge (a half-line) or a whole unbounded face.

The concept of infinite tetrahedron and, more generally, of infinite simplices, was introduced in [5]. For the sake of clarity, we recall here this concept in 3D configurations. Given four non-coplanar points \mathbf{a}_0 , \mathbf{a}_1 , \mathbf{a}_2 and \mathbf{a}_3 of the euclidian affine space \mathbb{R}^3 , define the infinite tetrahedon T whose vertices are \mathbf{a}_0 , \mathbf{a}_1 , \mathbf{a}_2 and \mathbf{a}_3 as the set of all the points \mathbf{x} which take the form

$$\mathbf{x} = \lambda_0 \mathbf{a}_0 + \lambda_1 \mathbf{a}_1 + \lambda_2 \mathbf{a}_2 + \lambda_3 \mathbf{a}_3, \quad \sum_{i=0}^3 \lambda_i = 1,$$

with $\lambda_0 \leq 0$, $\lambda_i \geq 0$ for $1 \leq i \leq 3$. It is usual to call \mathbf{a}_0 the fictitious vertex of T , while \mathbf{a}_1 , \mathbf{a}_2 and \mathbf{a}_3 are called the real vertices. It is worth noting that T is closed and convex. The tetrahedron S_T , associated to T , is the convex hull of the points \mathbf{a}_0 , \mathbf{a}_1 , \mathbf{a}_2 and \mathbf{a}_3 . The *altitude vector* of T is $\mathbf{h}_T = \pi_T \mathbf{a}_0 - \mathbf{a}_0$, where $\pi_T \mathbf{a}_0$ is the orthogonal projection of \mathbf{a}_0 on the affine plane containing \mathbf{a}_1 , \mathbf{a}_2 and \mathbf{a}_3 and separating T and S_T . Notice that

$$(28) \quad \forall \mathbf{x} \in T \cap S_T, \mathbf{h}_T \cdot (\mathbf{x} - \mathbf{a}_0) = |\mathbf{h}_T|^2.$$

Let us go back now to the decomposition (27). We should also note that M , the number

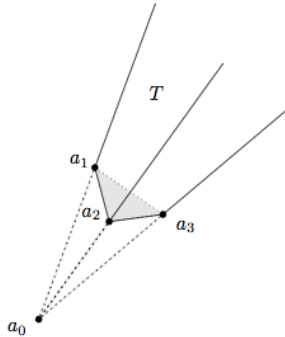


FIGURE 1. An example of an infinite tetrahedron.

of infinite tetrahedra, is not intended to be large. This is just a domain decomposition of a Ω_∞ in which the subdomains are infinite tetrahedra and are fixed once for all. In

practice, M is often small ($M = 3, 4, \dots$). An example is illustrated in Figure 3 where Ω_0 is a big tetrahedron centered at the origin and Ω_∞ is the union of 4 infinite tetrahedra (see also section 4 hereafter). Another possibility consists to choose Ω_0 as the octahedron $\{\mathbf{x} = (x_1, x_2, x_3) \in \mathbb{R}^3 \mid |x_1| + |x_2| + |x_3| < R\}$ and $\Omega_\infty = \mathbb{R}^3 \setminus \overline{\Omega_0}$ as the union of 8 infinite tetrahedra (see Figure 2). Subsequently, we denote by S_i , $1 \leq i \leq M$, the tetrahedron

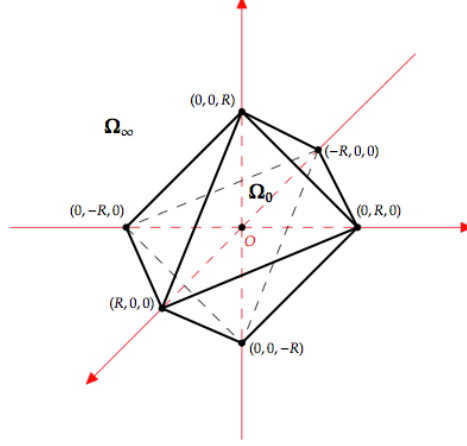


FIGURE 2. A decomposition of \mathbb{R}^3 in which Ω_0 is the octahedron $\{\mathbf{x} = (x_1, x_2, x_3) \in \mathbb{R}^3 \mid |x_1| + |x_2| + |x_3| < R\}$. Here Ω_∞ is the union of 8 infinite tetrahedra.

associated to T_i and by \mathbf{h}_i the altitude vector corresponding of T_i . We have

$$\overline{\Omega_0} \cap \overline{\Omega_\infty} = \cup_{i=1}^M (T_i \cap S_i).$$

Set

$$(29) \quad r_i(\mathbf{x}) = \frac{\mathbf{h}_i \cdot \mathbf{x}}{|\mathbf{h}_i|^2} \text{ for } \mathbf{x} \in S_i \cup T_i.$$

Since $\mathbf{0}$ is the fictitious vertex of each T_i and in view of (28) it can easily be proved that

$$r_i(\mathbf{x}) \geq 1 \text{ for } \mathbf{x} \in T_i, \quad r_i(\mathbf{x}) \leq 1 \text{ for } \mathbf{x} \in S_i, \quad \text{and } r_i(\mathbf{x}) = 1 \text{ for } \mathbf{x} \in T_i \cap S_i.$$

In terms of the local barycentric coordinates in S_i , $(\lambda_0^{(i)}, \lambda_1^{(i)}, \lambda_2^{(i)}, \lambda_3^{(i)})$, we can write

$$r_i(\mathbf{x}) = 1 - \lambda_0^{(i)}(\mathbf{x}) = \sum_{k=1}^3 \lambda_k^{(i)}(\mathbf{x}) \text{ for } \mathbf{x} \in T_i \cup S_i.$$

The following continuity property holds true: if T_i and T_j are neighbors, then

$$(30) \quad r_i(\mathbf{x}) = r_j(\mathbf{x}) \text{ for all } \mathbf{x} \in T_i \cap T_j.$$

The local polygonal inversion associated to T is defined as

$$(31) \quad \begin{aligned} \phi_i : (S_i \cup T_i) \setminus \{\mathbf{0}\} &\longrightarrow (S_i \cup T_i) \setminus \{\mathbf{0}\}, \\ \mathbf{x} &\longmapsto \frac{\mathbf{x}}{r_i(\mathbf{x})^2}. \end{aligned}$$

Obviously ϕ_i is a bijection between S_i and T_i . It is also an involution which preserves $T_i \cap S_i$, that is $\phi_i(\mathbf{x}) = \mathbf{x}$ for $\mathbf{x} \in T_i \cap S_i$.

Define now the *global polygonal inversion* ϕ from $\mathbb{R}^3 \setminus \{0\}$ into itself and the *global polygonal radius* $r(\cdot)$ as follows

$$r(\mathbf{x}) = r_i(\mathbf{x}) \text{ and } \phi(\mathbf{x}) = \phi_i(\mathbf{x}) \text{ for all } \mathbf{x} \in T_i \cup S_i, 1 \leq i \leq M.$$

In virtue of property (30), r and ϕ are well defined and *continuous* on \mathbb{R}^3 . Moreover, ϕ maps Ω_∞ into Ω_0 and conversely. We have

$$(32) \quad \phi(\mathbf{x}) = \mathbf{x} \text{ for all } \mathbf{x} \in \overline{\Omega_0} \cap \overline{\Omega_\infty}.$$

Moreover, there exists two constants $c_1 > 0$ and $c_2 > 0$ such that

$$c|\mathbf{x}| \leq r(\mathbf{x}) \leq c_2|\mathbf{x}| \text{ for all } \mathbf{x} \in \mathbb{R}^3,$$

In other words, $r(\mathbf{x}) \sim |\mathbf{x}|$ and $|\phi(\mathbf{x})| \sim |\mathbf{x}|^{-1}$ for $\mathbf{x} \in \mathbb{R}^3$. In the sequel, Ω_\star stands for the image of Ω_∞ by the inversion ϕ . From a strictly mathematical point of view $\Omega_\star = \Omega_0 \setminus \{\mathbf{0}\}$. However, since Ω_0 and Ω_\star will be meshed differently. We will therefore deal with them separately.

We now consider a family of pairs of triangulations $(\mathcal{T}_h, \mathcal{T}_h^\star)_h$ where

- $(\mathcal{T}_h)_h$ are regular triangulations of Ω_0 satisfying the usual conformity assumptions (see [5] or [7]). In particular, elements of \mathcal{T}_h are supposed shape regular in the usual sense: there exists a constant $c_0 > 0$ not depending on h such that

$$(33) \quad \max_{K \in \mathcal{T}_h \cup \mathcal{T}_h^\star} \frac{h_K}{\rho_K} \leq c_0.$$

Here h_K and ρ_K are respectively the diameter of K and the diameter of the sphere inscribed inside of the tetrahedron K .

- $(\mathcal{T}_h^\star)_h$ are regular triangulations of Ω_\star which satisfies, besides (33), the following additional requirement:
 - for each $K_\star \in \mathcal{T}_h^\star$, there exists $i \leq M$ such that $K_\star \subset S_i$ (in other words, \mathcal{T}_h^\star is a conforming union of triangulations of the subdomains S_1, \dots, S_M).
 - the triangulations $(\mathcal{T}_h^\star)_h$ are μ -graded, where $\mu \in (0, 1]$ is a fixed parameter. That means that there exists three constants $c_1^\star > 0$, $c_2^\star > 0$ and $c_3^\star > 0$, not depending on h , such that

$$(34) \quad \max_{K \in \mathcal{T}_h^{\star\star}} \frac{h_K}{d_K^{1-\mu}} \leq c_1^\star h,$$

$$(35) \quad \max_{K \in \mathcal{T}_h^\star \setminus \mathcal{T}_h^{\star\star}} h_K \leq c_2^\star h^{1/\mu},$$

$$(36) \quad \min_{K_\star \in \mathcal{T}_h^{\star\star}} d_{K_\star} \geq c_3^\star h^{1/\mu},$$

where $\mathcal{T}_h^{\star\star} = \{K \in \mathcal{T}_h^\star \mid \mathbf{0} \notin K\}$ (elements not touching the origin), $d_K = \inf_{\mathbf{x} \in K} |\mathbf{x}|$ for all $K \in \mathcal{T}_h^\star$, and

$$h = h(\mathcal{T}_h, \mathcal{T}_h^\star) = \max_{K \in \mathcal{T}_h \cup \mathcal{T}_h^\star} h_K,$$

Conditions (34), (35) and (36) mean that tetrahedra of \mathcal{T}_h^\star which are adjacent to $\partial\Omega_\star \cap \partial\Omega_\infty$ have a size of order h , while those touching the fictitious vertex $\mathbf{0}$ have a size of order $h^{1/\mu}$. Construction of graded meshes is detailed in [5].

- \mathcal{T}_h and \mathcal{T}_h^\star have the same vertices, edges and faces on the common boundary $\Omega_0 \cap \Omega_\infty = \partial\Omega_0 = \partial\Omega_\star \setminus \{\mathbf{0}\}$.

In the sequel, given a function v defined over Ω_∞ , \hat{v} stands for the function defined on Ω_\star as follows

$$(37) \quad \hat{v}(\mathbf{x}_\star) = \frac{1}{r(\mathbf{x}_\star)^\gamma} v(\phi(\mathbf{x}_\star)), \text{ for } \mathbf{x}_\star \in \Omega_\star.$$

with $\gamma > 0$ a parameter. Conversely, we have

$$(38) \quad v(\mathbf{x}) = \frac{1}{r(\mathbf{x})^\gamma} \hat{v}(\phi(\mathbf{x})), \quad \text{for } \mathbf{x} \in \Omega_\infty.$$

Now, let $k \geq 1$ be a fixed integer and consider the finite dimensional space

$$W_h = \{v \in \mathcal{C}^0(\mathbb{R}^3) \mid \forall K \in \mathcal{T}_h, v|_K \in (\mathbb{P}_k)^3; \forall K^* \in \mathcal{T}_h^*, \hat{v}|_{K^*} \in (\mathbb{P}_k)^3, \hat{v}(\mathbf{0}) = 0\}.$$

We may observe that functions of W_h are piecewise polynomial in the FEM region Ω_0 , but not in the IFEM region Ω_∞ . The last observation is due to distortion resulting from the composition with the inversion and the multiplicative factor involved in formula (37). Another observation concerns the behavior at large distances of functions belonging to W_h . Let $v \in W_h$. Then, $v \in H_{loc}^1(\mathbb{R}^3)^3$. Moreover, since $\hat{v}(\mathbf{0}) = 0$, we have

$$|\hat{v}(\mathbf{x}_*)| \leq C_0 |\mathbf{x}_*|, \quad \text{for all } \mathbf{x}_* \in \Omega_*,$$

for some constant C_0 , not depending on \mathbf{x}_* . It follows that for all $\mathbf{x} \in \Omega_\infty$, we have

$$|v(\mathbf{x})| = |r(\mathbf{x})|^{-\gamma} |\hat{v}(\phi(\mathbf{x}))| \leq C |\mathbf{x}|^{-\gamma} |\phi(\mathbf{x})| \leq C |\mathbf{x}|^{-\gamma-1}.$$

In similar way, we prove that

$$|\nabla v(\mathbf{x})| \leq C |\mathbf{x}|^{-\gamma-2}.$$

We deduce this

$$(39) \quad \gamma > -\frac{1}{2} \implies W_h \hookrightarrow W_0^1(\mathbb{R}^3)^3.$$

This justifies the following assumption on γ :

$$(40) \quad \gamma > -\frac{1}{2}.$$

The discrete problem writes: find $u_h \in W_h$ such that

$$(41) \quad \forall w_h \in W_h, \int_{\mathbb{R}^3} \nabla u_h \cdot \nabla w_h dx = \int_{\Omega} \mathbf{M} \cdot \nabla w_h dx.$$

The corresponding stray-field energy is given by

$$(42) \quad \mathcal{E}_{sf}(u_h) = \int_{\mathbb{R}^3} |\nabla u_h|^2 dx = \int_{\Omega} \mathbf{M} \cdot \nabla u_h dx.$$

We have

Proposition 3.1. *The discrete problem (41) has one and only one solution $u_h \in W_h$ and $\mathcal{E}_{sf}(u_h) \leq \mathcal{E}_{sf}(u)$. If in addition, $\gamma > 0$ and $u \in W_{k+\gamma}^{k+1}(\mathbb{R}^3)$, then*

$$(43) \quad \|u - u_h\|_{W_0^1(\mathbb{R}^3)^3} \leq C_1 h^{\tau k} \|u\|_{W_{k+\gamma}^{k+1}(\mathbb{R}^3)^3},$$

$$(44) \quad 0 \leq \mathcal{E}_{sf}(u) - \mathcal{E}_{sf}(u_h) \leq C_2 h^{\tau k} \|\mathbf{M}\|_{L^2(\Omega)} \|u\|_{W_{k+\gamma}^{k+1}(\mathbb{R}^3)^3},$$

where C_1 and C_2 are two constants not depending on h , \mathbf{M} and u , and

$$(45) \quad \tau = \min\left(\frac{\gamma}{\mu k}, 1\right).$$

Proposition 3.1 states in particular that if $u \in W_{k+\gamma}^{k+1}(\mathbb{R}^3)$ and if the mesh of Ω_* is graded enough ($\mu \leq \frac{\gamma}{k}$), then the error is similar to that held in the finite element method in bounded domains, that is

$$(46) \quad \|u - u_h\|_{W_0^1(\mathbb{R}^3)^3} \leq Ch^k \|u\|_{W_{k+\gamma}^{k+1}(\mathbb{R}^3)^3}.$$

We also have

$$(47) \quad 0 \leq \mathcal{E}_{sf}(u) - \mathcal{E}_{sf}(u_h) \leq C_2 h^k \|\mathbf{M}\|_{L^2(\Omega)} \|u\|_{W_{k+\gamma}^{k+1}(\mathbb{R}^3)^3}.$$

When smoothness of u is only local, we have this

Proposition 3.2. *Assume $u|_{\mathbb{R}^3 \setminus \bar{\Omega}} \in W_{k+\gamma}^{k+1}(\mathbb{R}^3 \setminus \bar{\Omega})$ and $u|_{\Omega} \in H^{k+1}(\Omega)$. Assume also that $\Omega \subset \Omega_0$ and that $\mathcal{T}_h|_{\Omega}$ is a triangulation of Ω . Then,*

$$(48) \quad \|u - u_h\|_{W_0^1(\mathbb{R}^3)^3} \leq C_1 (h^{\tau k} \|u\|_{W_{k+\gamma}^{k+1}(\Omega_\infty)} + h^k \|u\|_{H^{k+1}(\Omega)} + h^k \|u\|_{H^{k+1}(\Omega_0 \setminus \bar{\Omega})}),$$

$$(49)$$

$$0 \leq \mathcal{E}_{sf}(u) - \mathcal{E}_{sf}(u_h) \leq C_2 \|\mathbf{M}\|_{L^2(\Omega)} (h^{\tau k} \|u\|_{W_{k+\gamma}^{k+1}(\Omega_\infty)} + h^k \|u\|_{H^{k+1}(\Omega)} + h^k \|u\|_{H^{k+1}(\Omega_0 \setminus \bar{\Omega})}).$$

with τ given by (45).

From Proposition 2.4, we know that if $\operatorname{div} \mathbf{M} \in L^2(\Omega)$ and $\mathbf{M} \cdot \mathbf{n} \in H^{1/2}(\partial\Omega)$, then $u|_{\mathbb{R}^3 \setminus \bar{\Omega}} \in W_2^2(\mathbb{R}^3 \setminus \bar{\Omega})$ and $u|_{\Omega} \in H^2(\Omega)$. With $k = 1$ (P1 like elements) and $\gamma = 1$, we get the error estimate

$$(50) \quad \|u - u_h\|_{W_0^1(\mathbb{R}^3)^3} \leq Ch (\|u\|_{W_2^2(\mathbb{R}^3 \setminus \bar{\Omega})} + \|u\|_{H^2(\Omega)}),$$

$$(51) \quad 0 \leq \mathcal{E}_{sf}(u) - \mathcal{E}_{sf}(u_h) \leq C_2 \|\mathbf{M}\|_{L^2(\Omega)} h (\|u\|_{W_2^2(\mathbb{R}^3 \setminus \bar{\Omega})} + \|u\|_{H^2(\Omega)}),$$

for any $\mu \in (0, 1]$. This estimate is similar to the usual finite element error for elliptic problems in bounded domain.

PROOF OF PROPOSITIONS 3.1 AND 3.2 – Observe first that u is also solution of the minimization problem

$$\min_{v \in W_0^1(\mathbb{R}^3)^3} F(v), \quad \text{with } F(v) = \frac{1}{2} \int_{\mathbb{R}^3} |\nabla v|^2 - \int_{\mathbb{R}^3} \mathbf{M} \cdot \nabla v dx,$$

and, by virtue of (16), we have

$$F(u) = -\frac{1}{2} \int_{\mathbb{R}^3} |\nabla u|^2 dx = -\mathcal{E}_{sf}(\mathbf{M}),$$

Similarly, the approximate solution u_h is solution of

$$\min_{v_h \in W_h} F(v_h),$$

and, in view of (41), we have

$$F(u_h) = -\frac{1}{2} \int_{\mathbb{R}^3} |\nabla u_h|^2 dx = -\mathcal{E}_{sf}(u_h),$$

Since $W_h \subset W_0^1(\mathbb{R}^3)^3$, we deduce that $F(u_h) \geq F(u)$. Thus, $\mathcal{E}_{sf}(u_h) \leq \mathcal{E}_{sf}(u)$.

Now, Céa's lemma gives

$$\|u - u_h\|_{W_0^1(\mathbb{R}^3)^3} \leq C_1 \inf_{w_h \in W_h} \|u - w_h\|_{W_0^1(\mathbb{R}^3)^3}.$$

for some constant C_1 not depending on u nor on h . In [5], the following estimate is proven:

$$\inf_{w_h \in W_h} \|u - w_h\|_{W_0^1(\mathbb{R}^3)^3}^2 \leq C (h^{2\tau k} \|u\|_{W_{k+\gamma}^{k+1}(\Omega_\infty)}^2 + h^{2k} \sum_{K \in \mathcal{T}_h} \|u\|_{H^{k+1}(K)}^2).$$

We easily get estimate (43) and (48). In addition, we have

$$0 \leq \mathcal{E}_{sf}(u) - \mathcal{E}_{sf}(u_h) = \frac{1}{2} \int_{\mathbb{R}^3} |\nabla u|^2 dx - \frac{1}{2} \int_{\mathbb{R}^3} |\nabla u_h|^2 dx = \frac{1}{2} \int_{\mathbb{R}^3} \mathbf{M} \cdot (\nabla u - \nabla u_h) dx.$$

Thus,

$$\mathcal{E}_{sf}(u) - \mathcal{E}_{sf}(u_h) \leq \frac{1}{2} \|\mathbf{M}\|_{L^2(\Omega)} \cdot \|\nabla u - \nabla u_h\|_{L^2(\Omega)}.$$

Combining with (43) gives (44). Estimates (48) and (49) are obtained by the same argument. ■

4. NUMERICAL RESULTS

The task of this section is to show some numerical results obtained with a 3D code writing for solving (4) with the following parameters: $k = 1$ (P1 like elements). We use the following domain decomposition of \mathbb{R}^3 :

- Ω_0 is the (big) tetrahedra whose vertices are

$$(52) \quad \begin{aligned} \mathbf{a}_1 &= R_0 \left(\frac{\sqrt{8}}{3}, 0, -\frac{1}{3} \right), & \mathbf{a}_2 &= R_0 \left(-\frac{\sqrt{2}}{3}, \sqrt{\frac{2}{3}}, -\frac{1}{3} \right), \\ \mathbf{a}_3 &= R_0 \left(-\frac{\sqrt{2}}{3}, -\sqrt{\frac{2}{3}}, -\frac{1}{3} \right), & \mathbf{a}_4 &= R_0(0, 0, 1), \end{aligned}$$

where $R_0 > 0$ is a size parameter (see Figure 3).

- $\Omega_\infty = \mathbb{R}^3 \setminus \overline{\Omega}_0$ is decomposed as the union of four infinite simplices T_i , $1 \leq i \leq 4$, with the origin as a common fictitious vertex. The three real vertices T_i , $1 \leq i \leq 4$, are $(\mathbf{a}_j)_{1 \leq j \neq i \leq 4}$ (the bounded faces of T_i , $1 \leq i \leq 4$, are the faces of Ω_0).

The code we write does not depend on the considered configuration. It only requires that $\Omega \subset \Omega_0$. In all the tests, we choose

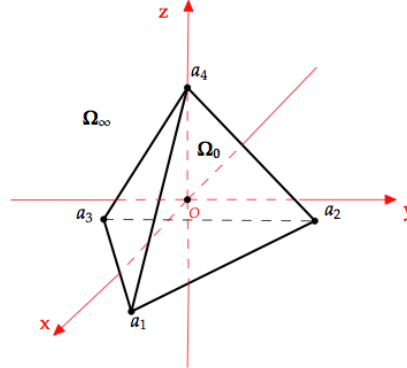


FIGURE 3. The decomposition $\mathbb{R}^3 = \overline{\Omega}_\infty \cup \overline{\Omega}_0$ is used in implementation. Here $\overline{\Omega}_0$ is a big tetrahedron whose vertices are given by formula (52).

Numerical example 1 (homogeneously magnetized sphere). We consider the case of a ball $\Omega = \{\mathbf{x} \in \mathbb{R}^3 \mid |\mathbf{x}| < r_0\}$. If \mathbf{M} is constant, that is $\mathbf{M} = \mathbf{M}_0$ for some unit vector field $\mathbf{M}_0 \in \mathbb{R}^3$, then the solution of (4) is given by

$$(53) \quad u(\mathbf{x}) = \begin{cases} \frac{1}{3} \mathbf{M}_0 \cdot \mathbf{x} & \text{if } |\mathbf{x}| < r_0, \\ \frac{r_0^3}{3} \frac{\mathbf{M}_0 \cdot \mathbf{x}}{|\mathbf{x}|^3} & \text{if } |\mathbf{x}| \geq r_0. \end{cases}$$

In computational tests, we choose $\mathbf{M}_0 = (0, 0, 1)$, $r_0 = 0.5$ and $R_0 = 4$. In order to check the convergence of the method, we measure the following errors

$$e_0(u) = \frac{\|u_h - u\|_{W_{-1}^0(\mathbb{R}^3)}}{\|u\|_{W_{-1}^0(\mathbb{R}^3)}}, \quad e(\mathcal{E}_{sf}) = \frac{|\mathcal{E}_{sf}(u) - \mathcal{E}_{sf}(u_h)|}{|\mathcal{E}_{sf}(u)|}.$$

In the context of this example, the exact energy is given by

$$(54) \quad \mathcal{E}_{sf}(u) = \frac{1}{2} \int_{\mathbb{R}^3} |\nabla u|^2 dx = -\frac{1}{2} \int_{\Omega} \mathbf{M}_0 \cdot \mathbf{h} dx = \frac{2\pi |\mathbf{M}_0|^2}{9} r_0^3 = 0.08723.$$

Obviously, $u|_{\Omega} \in H^2(\Omega)$. One can also check that $u|_{\mathbb{R}^3 \setminus \bar{\Omega}} \in W_2^2(\mathbb{R}^3 \setminus \bar{\Omega})$. However, $u \notin W_2^2(\mathbb{R}^3)$ since $[\frac{\partial u}{\partial n}] = -\mathbf{M}_0 \cdot \mathbf{n} \neq 0$ on $\partial\Omega$. According to estimates (51) and (51) errors $e_0(u)$ and $e(\mathcal{E}_{sf})$ decrease as h (for any gradation parameter μ). Table 1 and Figure 4 display these errors versus h for several values of μ . We may observe that $e_0(u)$ decreases as $h^{0.96}$ while $e(\mathcal{E}_{sf})$ decreases as $h^{1.33}$. The errors are essentially the same for $\mu = 1$, $\mu = 0.7$ and $\mu = 0.5$. This is in accordance with estimates (50) and (51). In Figure 5 the approximate solution and the exact one are displayed versus r when $x = y = 0$. It can be seen by a visual comparison that these solutions are very close although the discontinuity of the normal component of $\mathbf{h} = -\nabla u$ across the interface $\partial\Omega$.

DoF	h	μ			μ		
		1	0.7	0.5	1	0.75	0.5
		$e_0(u)$			$e(\mathcal{E}_{sf})$ (energy error)		
875	1.131	0.292	0.284	0.280	0.532	0.523	0.517
6750	0.565	0.145	0.139	0.135	0.322	0.315	0.312
22625	0.377	0.101	0.098	0.097	0.157	0.152	0.150
53500	0.282	0.076	0.074	0.073	0.127	0.124	0.123
104375	0.226	0.064	0.062	0.062	0.089	0.086	0.085
180250	0.188	0.052	0.051	0.051	0.073	0.072	0.071
427000	0.141	0.040	0.039	0.039	0.043	0.042	0.041
833750	0.113	0.032	0.031	0.031	0.025	0.024	0.024
The log. slope		0.96	0.96	0.96	1.33	1.34	1.33

TABLE 1. (Example 1) The relative errors $e_0(u)$ and $e(\mathcal{E}_{sf})$ ($r_0 = 0.5$, $\gamma = 1$, and $R_0 = 4$).

4.1. Numerical example 2 (non homogeneously magnetized sphere). In this second example, we consider the case of a non homogeneous magnetization of a sphere $\Omega = \{\mathbf{x} \in \mathbb{R}^3 \mid |\mathbf{x}| < r_0\}$. More precisely, \mathbf{M} is the unit vector field

$$(55) \quad \mathbf{M} = (\cos \theta) \mathbf{e}_\varphi + (\sin \theta) \mathbf{e}_\theta \text{ in } \Omega.$$

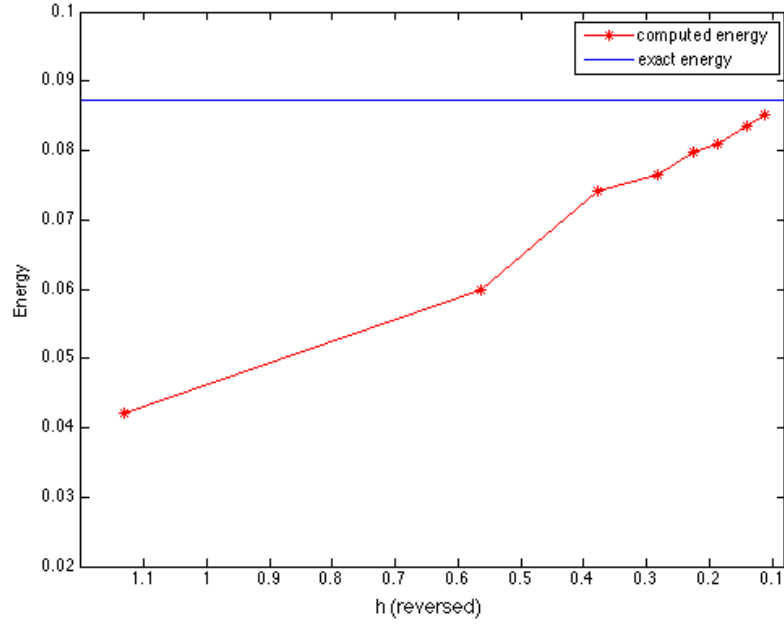


FIGURE 4. (Example 1) the exact and the approximate energy versus h with $\mu = 0.5$, $\gamma = 1$, $R_0 = 4$ and $r_0 = 0.5$.

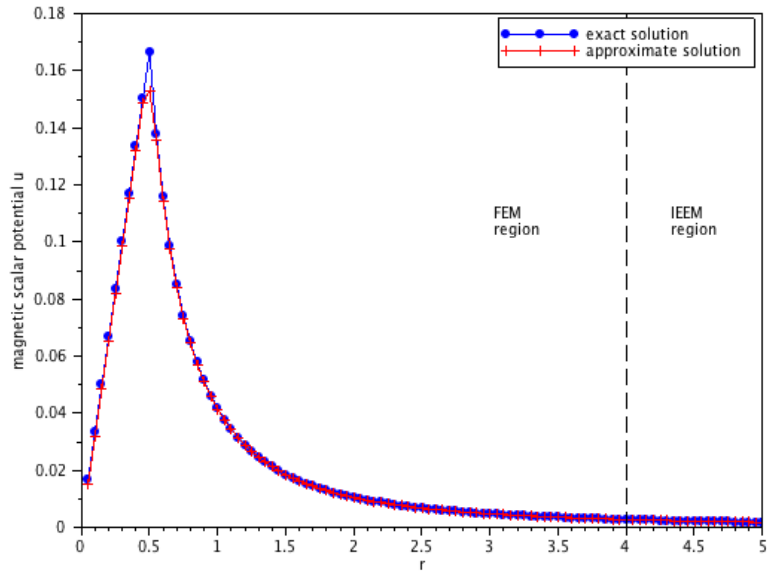


FIGURE 5. (Example 1) the exact and the approximate scalar potential versus $r = |\mathbf{x}|$ when $x = y = 0$ and $z \geq 0$ ($\mu = 0.5$, $\gamma = 1$, $R_0 = 4$, $r_0 = 0.5$ and $DoF = 833750$).

Here (r, φ, θ) , $r \geq 0$, $0 \leq \varphi \leq 2\pi$, $0 \leq \theta \leq \pi$, denote the spherical coordinates and $(\mathbf{e}_r, \mathbf{e}_\varphi, \mathbf{e}_\theta)$ the corresponding unit vectors. In that case, the solution can be obtained

explicitly (see the appendix):

$$(56) \quad u(\mathbf{x}) = \begin{cases} -\frac{2z}{9} + \frac{2z}{3} \ln\left(\frac{|\mathbf{x}|}{r_0}\right) & \text{if } |\mathbf{x}| \leq r_0, \\ -\frac{2r_0^3 z}{9|\mathbf{x}|^3} & \text{if } |\mathbf{x}| \geq r_0. \end{cases}$$

This solution belongs to $W_2^2(\mathbb{R}^3)$, as forecasted in Proposition 2.4 (indeed, $\operatorname{div} \mathbf{M} \in L^2(\Omega)$ and $\mathbf{M} \cdot \mathbf{n} = 0$ on $\partial\Omega$). In our numerical experiences, we fixe $r_0 = 0.5$ and $R_0 = 6$. The exact stray-field energy is given by

$$(57) \quad \mathcal{E}_{sf}(u) = \frac{1}{2} \int_{\mathbb{R}^3} |\nabla u|^2 dx = \frac{16}{81} \pi r_0^3 = 0.0776.$$

According to Proposition 2.4, no gradation is needed to get optimal convergence. More precisely, estimates (46) and (47) hold true for any gradation paramater $\mu \leq 1$ (here $k = 1$ and $\gamma = 1$), that is

$$(58) \quad \|u - u_h\|_{W_0^1(\mathbb{R}^3)^3} \leq Ch \|u\|_{W_2^2(\mathbb{R}^3)^3},$$

$$(59) \quad 0 \leq \mathcal{E}_{sf}(u) - \mathcal{E}_{sf}(u_h) \leq C_2 h \|u\|_{W_2^2(\mathbb{R}^3)^3}.$$

Table 2 shows these relative errors versus h . The behavior of the discrete stray-field energy $\mathcal{E}_{sf}(\mathbf{M})$ is also displayed in Figure 6, while the approximate and the exact solutions are displayed versus $r = |\mathbf{x}|$ in Figure 7 (when $x = y = z$). We can observe that the energy converges as $h^{2.5}$. This superconvergence of energy is not foreseen in estimate (44) and has not been proved. We conjecture that this superconvergence of the energy holds when $u \in W_2^2(\mathbb{R}^3)$ (or, equivalently, when $\mathbf{M} \in H(\operatorname{div}; \Omega)$ and $\mathbf{M} \cdot \mathbf{n} = 0$ on $\partial\Omega$).

DoF	h	μ			μ		
		1	0.7	0.5	1	0.75	0.5
		$e_0(u)$			$e(\mathcal{E}_{sf})$		
875	1.131	0.258	0.250	0.247	0.623	0.619	0.615
6750	0.565	0.153	0.149	0.148	0.325	0.322	0.320
22625	0.377	0.101	0.099	0.099	0.151	0.149	0.148
53500	0.282	0.073	0.072	0.071	0.084	0.083	0.082
104375	0.226	0.061	0.060	0.059	0.054	0.053	0.052
180250	0.188	0.049	0.048	0.048	0.033	0.032	0.032
427000	0.141	0.037	0.036	0.036	0.009	0.008	0.008
833750	0.113	0.029	0.029	0.029	0.001	0.002	0.002
The log. slope		0.95	0.94	0.93	2.79	2.49	2.49

TABLE 2. (Example 2) The relative errors $e_0(u)$ and $e(\mathcal{E}_{sf})$ ($\gamma = 1$, $R_0 = 6$ and $r_0 = 0.5$).

Numerical example 3. As a last benchmark, we consider a homogeneously magnetized unit cube: $\mathbf{M} = (0, 0, 1)$ and $\Omega = [-1/2, 1/2]^3$ (see, e. g., [8]). The stray-field energy in this case is given by

$$(60) \quad \mathcal{E}_{sf}(u) = \frac{1}{6}.$$

In Table 3, error on the energy versus h is displayed for several values of μ . In figure 8, we show the evolution of the energy versus h . Here also we may observe that the approximate energy converges quickly to the exact one. This superconvergence can clearly be seen in Figure 8.

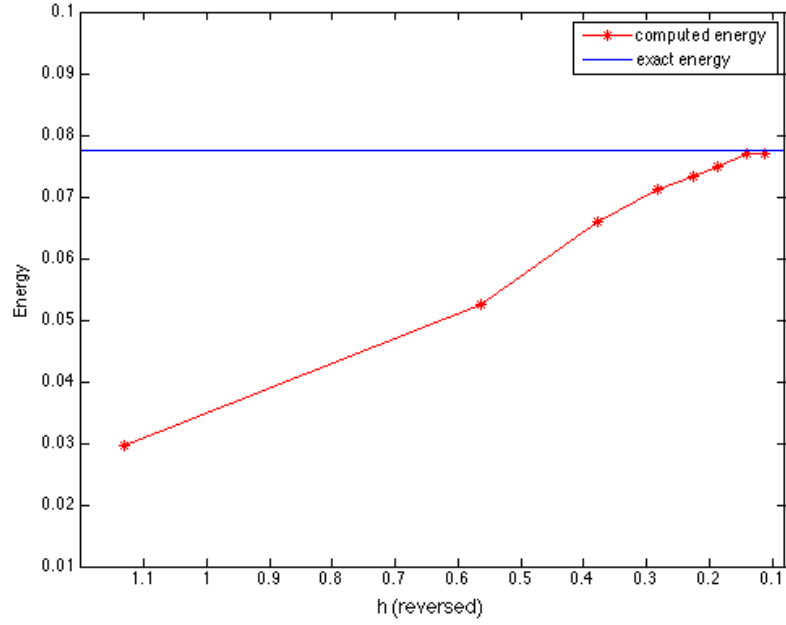


FIGURE 6. (Example 2) The exact and the approximate energy versus h with $\mu = 0.5$, $r_0 = 0.5$, $\gamma = 1$ and $R_0 = 6$.

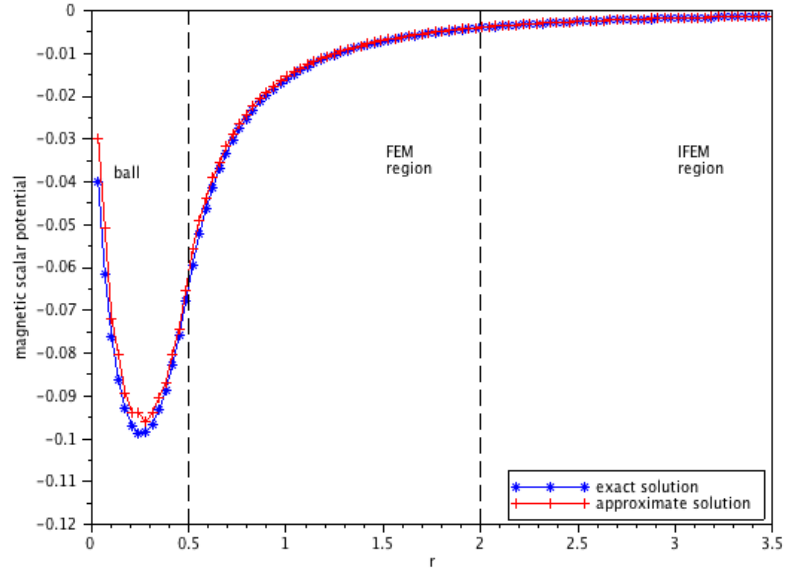


FIGURE 7. (Example 2) The exact and approximate magnetic scalar potential versus $r = |\mathbf{x}|$ (with $x = y = z$). Here $\mu = 0.5$, $\gamma = 1$, $R_0 = 6$ and $DoF = 833750$.

DOF	h	The relative error of energy		
		μ		
		1	0.7	0.5
875	1.697	0.468	0.463	0.460
6750	0.848	0.364	0.360	0.358
22625	0.565	0.298	0.295	0.294
53500	0.424	0.243	0.241	0.240
104375	0.339	0.205	0.203	0.203
180250	0.282	0.134	0.133	0.133
427000	0.212	0.013	0.013	0.012

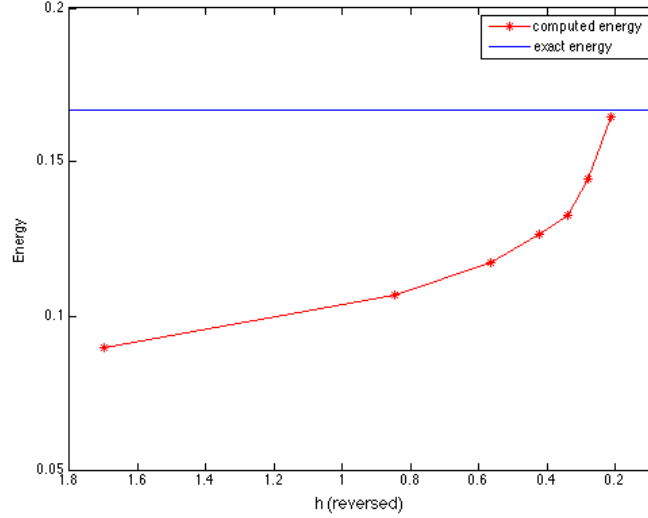
 TABLE 3. The relative error of energy for $\gamma = 1$ (example 3)


FIGURE 8. (Example 3) The computed energy of an homogeneously magnetized unit cube.

APPENDIX A. SOLVING THE PROBLEM IN THE CASE OF AN INHOMOGENEOUSLY MAGNETIZED BALL (NUMERICAL EXAMPLE 2)

The resolution of the system in the case of a ball B_{r_0} and \mathbf{M} given by (55) can be done by means of a decomposition on spherical harmonics $(Y_\ell^m)_{\ell \geq 0, -\ell \leq m \leq \ell}$ (which is orthonormal with respect to the inner product in $L^2(\mathbb{S}^2)$). We have outside the ball B_{r_0} :

$$\Delta u = 0 \text{ in } \mathbb{R}^3 \setminus \overline{B_{r_0}}.$$

Developping u on the basis of spherical harmonics gives (see, e. g., [19]):

$$u(\mathbf{x}) = \sum_{\ell=0}^{+\infty} \sum_{m=-\ell}^{\ell} A_\ell^m \left(\frac{r}{r_0} \right)^{-\ell-1} Y_\ell^m(\varphi, \theta).$$

where $(A_\ell^m)_{\ell \geq 0, -\ell \leq m \leq \ell}$ is a sequence of complex coefficients. On the other hand, we have in the interior of the ball

$$\Delta u = \operatorname{div} \mathbf{M} = 2 \frac{\cos \theta}{r} = \frac{\alpha}{r} Y_1^0(\varphi, \theta) \text{ in } \overline{B_{r_0}}, \quad \text{with } \alpha = 4\sqrt{\frac{\pi}{3}}.$$

Writing

$$u(\mathbf{x}) = \sum_{\ell=0}^{+\infty} \sum_{m=-\ell}^{\ell} u_{\ell}^m(r) Y_{\ell}^m(\varphi, \theta), \text{ in } \overline{B}_{r_0},$$

gives:

$$\frac{1}{r^2} \frac{d}{dr} \left(r^2 \frac{du_{\ell}^m}{dr} \right) (r) - \frac{\ell(\ell+1)}{r^2} u_{\ell}^m(r) = \frac{\alpha}{r} \delta_{\ell,1} \delta_{m,0} \text{ for all } \ell \geq 0 \text{ and } -\ell \leq m \leq \ell,$$

where $\delta_{i,j}$, $i \in \mathbb{N}$, $j \in \mathbb{N}$, denotes the usual Kronecker delta. The solutions of this equations are of the form

$$u_{\ell}^m(r) = B_{\ell}^m \left(\frac{r}{r_0} \right)^{\ell} + C_{\ell}^m \left(\frac{r}{r_0} \right)^{-\ell-1} + \frac{\alpha}{3} r \ln\left(\frac{r}{r_0}\right) \delta_{\ell,1} \delta_{m,0},$$

where B_{ℓ}^m and C_{ℓ}^m are constants. Since $u \in W_0^1(\mathbb{R}^3)$ we deduce that $u_{B_{r_0}} \in H^1(B_{r_0})$. Necessarily $C_{\ell}^m = 0$ for all $\ell \geq 0$ and $|m| \leq \ell$. Since $[u]_{\partial\Omega} = 0$, we deduce that $B_{\ell}^m = A_{\ell}^m$ for all $\ell \geq 0$ and $|m| \leq \ell$. In addition,

$$\left[\frac{\partial u}{\partial r} \right]_{\partial\Omega} = -\mathbf{M} \cdot \mathbf{n} = -\mathbf{M} \cdot \mathbf{e}_r = 0.$$

Thus, for all $\ell \geq 0$ and $|m| \leq \ell$ we have

$$\ell \frac{B_{\ell}^m}{r_0} + \frac{\alpha}{3} \delta_{\ell,1} \delta_{m,0} = -\frac{\ell+1}{r_0} A_{\ell}^m.$$

Thus, $A_{\ell}^m = B_{\ell}^m = 0$ for $(\ell, m) \neq (1, 0)$ and

$$A_1^0 = B_1^0 = -\frac{\alpha r_0}{9}.$$

Thus, if $|\mathbf{x}| \geq r_0$ then

$$u(\mathbf{x}) = A_1^0 \left(\frac{r_0}{r} \right)^2 Y_1^0 = -\frac{r_0^3}{9r^2} \alpha Y_1^0 = -\frac{2r_0^3 \cos \theta}{9r^2} = -\frac{2r_0^3 z}{9r^3}.$$

and

$$\|\nabla u\|_{L^2(\mathbb{R}^3 \setminus \overline{B}_{r_0})}^2 = \frac{32\pi}{243} r_0^3.$$

If $|\mathbf{x}| \leq r_0$ then

$$u(\mathbf{x}) = \left(B_1^0 \frac{r}{r_0} + \frac{\alpha}{3} r \ln\left(\frac{r}{r_0}\right) \right) Y_1^0 = \left(-\frac{r}{9} + \frac{r}{3} \ln\left(\frac{r}{r_0}\right) \right) \alpha Y_1^0 = \frac{2r \cos \theta}{9} (-1 + 3 \ln\left(\frac{r}{r_0}\right)).$$

Thus,

$$u = \frac{2z}{9} (-1 + 3 \ln\left(\frac{r}{r_0}\right)),$$

and

$$\|\nabla u\|_{L^2(\overline{B}_{r_0})}^2 = \frac{64\pi}{243} r_0^3.$$

Thus, the energy of the corresponding stray-field is

$$\mathcal{E}_{sf}(u) = \frac{1}{2} \int_{r_0^3} |\nabla u|^2 dx = \frac{16}{81} \pi r_0^3.$$

Aknowlegement.

This work was partially supported by a public grant as part of the Investissement d'avenir project, reference ANR-11-LABX-0056-LMH, LabEx LMH.

Declarations.

Conflict of interest: The authors declare no competing interests.

REFERENCES

- [1] F. Alliot. *Etude des équations stationnaires de Stokes et Navier-Stokes dans des domaines extérieurs*. PhD Thesis, ENPC, Paris, 1998.
- [2] C. Amrouche, V. Girault, and J. Giroire. Weighted Sobolev spaces for Laplace's equation in \mathbf{R}^n . *J. Math. Pures Appl. (9)*, 73(6):579–606, 1994.
- [3] D. V. Berkov, K. Ramstöck, and A. Hubert. Solving micromagnetic problems: toward an optimal numerical method. *Phys. Stat. Sol (a)*, 137:207–225, 1993.
- [4] J. L. Blue and M. R. Scheinfein. Using multipoles decreases computation time for magnetic self-energy. *IEEE Trans. Magn.*, 27:4778–4780, 1991.
- [5] T. Z. Boulmezaoud. Inverted finite elements: a new method for solving elliptic problems in unbounded domains. *M2AN Math. Model. Numer. Anal.*, 39(1):109–145, 2005.
- [6] C. Carstensen and A. Prohl. Numerical analysis of relaxed micromagnetics by penalised finite elements. *Numer. Math.*, 90(1):65–99, 2001.
- [7] Ph.-G. Ciarlet. *The finite element method for elliptic problems*. North-Holland Publishing Co., Amsterdam, 1978.
- [8] A. Class, L. Exl, G. Selke, A. Drews, and Th. Schrefl. Fast stray field computation on tensor grids. *Journal of magnetism and magnetic materials*, 176(326), 2013.
- [9] L. Exl, W. Auzinger, S. Bance, M. Gusenbauer, F. Reichel, and T. Schrefl. Fast stray field computation on tensor grids. *J. Comput. Phys.*, 231(7):2840–2850, 2012.
- [10] D. R. Fredkin and T. R. Koehler. Hybrid method for computing demagnetizing fields. *IEEE Trans. Magn.*, 26:415–417, 1990.
- [11] J. Giroire. *Etude de quelques problèmes aux limites extérieurs et résolution par équations intégrales*. Thèse de Doctorat d'Etat. Université Pierre et Marie Curie, Paris, 1987.
- [12] H. Han and W. Bao. The discrete artificial boundary condition on a polygonal artificial boundary for the exterior problem of Poisson equation by using the direct method of lines. *Comput. Methods Appl. Mech. Engrg.*, 179(3-4):345–360, 1999.
- [13] H. Han and W. Bao. Error estimates for the finite element approximation of problems in unbounded domains. *SIAM J. Numer. Anal.*, 37(4):1101–1119, 2000.
- [14] B. Hanouzet. Espaces de Sobolev avec poids application au problème de Dirichlet dans un demi-espace. *Rend. Sem. Mat. Univ. Padova*, 46:227–272, 1971.
- [15] T. R. Koehler and D. R. Fredkin. Finite element methods for micromagnetism. *IEEE Trans. Magn.*, 28:1239–1244, 1992.
- [16] S. Labbé. Fast computation for large magnetostatic systems adapted for micromagnetism. *SIAM J. Sci. Comput.*, 26(6):2160–2175, 2005.
- [17] H. Long, E. Ong, Z. Liu, and E. Li. Fast fourier transform on multipoles for rapid calculation of magnetostatic fields. *IEEE Trans. Magn.*, 42:295–300, 2006.
- [18] M. Luskin and L. Ma. Analysis of the finite element approximation of microstructure in micromagnetics. *SIAM J. Numer. Anal.*, 29(2):320–331, 1992.
- [19] J.-C. Nédélec. *Acoustic and electromagnetic equations*, volume 144 of *Applied Mathematical Sciences*. Springer-Verlag, New York, 2001. Integral representations for harmonic problems.
- [20] N. Popović and D. Praetorius. Applications of H -matrix techniques in micromagnetics. *Computing*, 74(3):177–204, 2005.
- [21] A. Prohl. *Computational micromagnetism*. Advances in Numerical Mathematics. B. G. Teubner, Stuttgart, 2001.